NIR photo-driven upconversion in NaYF$_4$:Yb,Er/PLGA particles for *in vitro* bioimaging of cancer cells

Lidija Mancic[a,*], Aleksandra Djukic-Vukovic[b], Ivana Dinic[c], Marko G. Nikolic[d], Mihailo D. Rabasovic[d], Aleksandar J. Krmpot[d], Antonio M.L.M. Costa[e], Dijana Trisic[f], Milos Lazarevic[g], Ljiljana Mojovic[b], Olivera Milosevic[a]

[a] *Institute of Technical Sciences of the Serbian Academy of Sciences and Arts, Belgrade, Serbia*
[b] *Department of Biochemical Engineering and Biotechnology, Faculty of Technology and Metallurgy, University of Belgrade, Serbia*
[c] *Innovation Center of the Faculty of Chemistry, University of Belgrade, Serbia*
[d] *Photonic Center, Institute of Physics Belgrade, University of Belgrade, Zemun, Belgrade, Serbia*
[e] *Department of Chemical and Materials Engineering, Pontifical Catholic University of Rio de Janeiro, Rio de Janeiro, Brazil*
[f] *Clinic for Pediatric and Preventive Dentistry, School of Dental Medicine, University of Belgrade, Serbia*
[g] *Institute of Human Genetics, School of Dental Medicine, University of Belgrade, Serbia*

ARTICLE INFO

ABSTRACT

Lanthanide-doped fluoride up-converting nanoparticles (UCNPs) represent the new class of imaging contrast agents which hold great potential for overcoming existing problems associated with traditionally used dyes, proteins and quantum dots. In this study, a new kind of hybrid NaYF$_4$:Yb,Er/PLGA nanoparticles for efficient biolabeling were prepared through one-pot solvothermal synthesis route. Morphological and structural characteristics of the as-designed particles were obtained using X-ray powder diffraction (XRPD), scanning and transmission electron microscopy (SEM/TEM), energy dispersive spectroscopy (EDS), Fourier transform infrared (FTIR) and photoluminescence (PL) spectroscopy, while their cytotoxicity as well as up-conversion (UC) labeling capability were tested *in vitro* toward human gingival cells (HGC) and oral squamous cell carcinoma (OSCC). The results revealed coexistence of the cubic (*Fm*-3*m*) and hexagonal (*P*6$_3$/*m*) phase in spherical and irregularly shaped nanoparticles, respectively. PLGA [Poly(lactic-*co*-glycolic acid)] ligands attached at the surface of UCNPs particles provide their enhanced cellular uptake and enable high-quality cells imaging through a near-infrared (NIR) laser scanning microscopy (λ_{ex} = 980 nm). Moreover, the fact that NaYF4:Yb,Er/PLGA UCNPs show low cytotoxicity against HGC over the whole concentration range (10–50 μg/mL) while a dose dependent viability of OSCC is obtained indicates that these might be a promising candidates for targeted cancer cell therapy.

1. Introduction

Head and neck cancers represent the sixth most common cancer worldwide, with the highest incidence rates in Melanesia, South-Central Asia and Central and Eastern Europe [1]. Among them, oral squamous cell carcinoma (OSCC) is the most common malignant epithelial neoplasm affecting the oral cavity. The incidence of oral cavity cancer appearance is higher in males and as the major risk factors are considered smoking, alcohol use, smokeless tobacco use and human papillomavirus (HPV). Early stages of disease are asymptomatic and very similar to other mucosal diseases and if diagnosed at advanced stages result with a 5-year survival rate of around 50%. Fatal outcomes are mostly caused by local recurrence and neck lymph node metastasis [2]. Therefore, advancements in both, early diagnosis and therapy, are

necessary and most likely will come from innovative non-invasive selective optical techniques [3]. Among the various optical diagnostic methods, fluorescence imaging is of immense importance since that provides accurate visualization of the molecular and functional processes in the human body [4].

Moreover, with the current progress in designing of the new hybrid multifunctional lanthanide-doped up-conversion nanoparticles (UCNPs) whose excitation/emission falls into the biological tissue transparency window, superior optical diagnostic and targeted drug delivery is expectable in the near future [5, 6]. Due to efficient two-phonon excitation and the large anti-Stocks shift UCNPs are able to emit visible or UV photons under excitation by near-infrared (NIR) light, to achieve deeper tissue penetration, and to exhibit higher photochemical stability in comparison with a traditionally used fluorophores [7]. The

effectiveness of these materials is principally dependent on the crystal structure and phonon energy of a host matrix, as well as, on the choice and concentration of lanthanide dopants. Efficient lanthanide pairs which can easily upconvert low energy photons into higher ones comprise ytterbium (Yb^{3+}) as a sensitizer and erbium (Er^{3+}), thulium (Tm^{3+}) or holmium (Ho^{3+}) as activator. The rich energy levels and long-lived intermediate excited states of activators provide various energy transfer pathways for UC emissions in visible spectra. Following initial Yb^{3+} excitation by 980 nm laser, energy transfer upconversion (ETU), excited state absorption (ESA), photon avalanche (PA), co-operative energy transfer (CET) and cross-relaxation (CR) processes take place determining resulting fluorescence efficiency of UCNPs [8]. Among many compounds, fluoride based cubic or hexagonal crystal lattices of $NaYF_4$ phase have been extensively studied as the most efficient hosts because of their low phonon energy (*i.e.*, 350 cm^{-1}), which minimize harmful non-radiative relaxations, and high optical transparence necessary for migration of NIR photons. In particular, hexagonal phase exhibits approximately one order of magnitude higher UC emission in comparison to cubic counterpart since it possess a higher degree of asymmetry, multisite occupation with lanthanide dopant ions and shorter distance among them. Since that particle size also affects the luminescence efficiency (higher energy transfer loss is attributed to the higher density of the surface defects) different synthesis strategies were developed to highlight tailored performances of specially designed core-shell, hybrid and composite UCNPs for cell imaging and tracking, drug delivery, photodynamic therapy and target recognition of biospecies [9, 10]. Although showing remarkable characteristics during both *in vitro* and *in vivo* investigations studied structures were usually obtain through complex multi-steps procedure which involves decomposition of organometallic compounds in oleic acid and subsequent ligand exchange (or oxidation, coating, intercalation, *etc.*). Usage of toxic and hazardous substances during synthesis raised deep concerns regarding potential toxicity of synthesized UCNPs [11–13]. Recently, it was shown that such obtained UCNPs could regain their cytotoxicity upon interaction with cells if weakly coordinated surface groups are used to render them biocompatible after synthesis [14]. Thus, the safe biological application of UCNPs implies establishing of facile and reliable procedure which would minimize the usage of toxic solvents and provide hydrophilic reactive surface *in situ* toward enhanced conjugation of proteins and drugs. One-pot polymer assisted hydrothermal approach, originally reported by Wang et al. [15] is a simple procedure which enables direct synthesis of water-dispersible UCNPs. To date, it was used for *in situ* functionalization of UCNPs surface with a wide range of biocompatible capping ligands, including carboxylic and amine/imine groups of polymers, such as: polyethylenimine (PEI), polyacrylic acid (PAA), polyvinylpyrrolidone (PVP) and polyethylene glycol (PEG) [16–18]. Among others, we have also shown that PVP-, PEG- and EDTA-assisted hydro/solvothermal route, performed in a controlled manner, led to the generation of hydrophilic/biocompatible upconverting particles with a different shape (spherical, rod, prisms, octahedron and desert-rose) [19, 20]. Here, we reported for the first time usages of poly(lactic-*co*-glycolic acid) (PLGA) *during* solvothermal synthesis of $NaYF_4$:Yb/Er nanoparticles. PLGA, approved by the United States Food and Drug Administration and European Medicine Agency for pharmaceutical application and human use, is one of the most widely utilized biodegradable polymer with a minimal toxicity associated with its use as scaffolds for tissue engineering or for delivery of macromolecular therapeutics [21–23]. For example, PLGA nanoparticles have been proposed as a delivery medium of an amphiphilic Gd^{3+} complex developed for the need of high sensitive magnetic resonance imaging (MRI) and imaging guided drug delivery applications [24]. Similarly, it was shown that pH-responsive PLGA(UCNPs/doxorubicin hydrochloride) nanocapsules obtained through self-assembly strategy could act as T1-weighted contrast agents MRI, cell imaging label and effective chemotherapy drug delivery system [25]. Due to fact that PLGA comprises both, hydrophilic and hydrophobic moiety, it was

usually used in combination with PEG in the form of amphiphilic block-copolymer for posterior UCNPs coating *via* flash nanoprecipitation. PEG-PLGA layer formed in such way provides excellent UCNPs colloidal stability in deionized water, buffers and serum media, but in the case of a thicker layer formation decrease of the upconversion luminescence was observed [26]. Recently, fabrication of a multifunctional nanovector for simultaneous gene delivery and real-time intracellular tracking based on UCNPs modified by positively charged amphiphilic polymer and PEG–PLGA copolymer was reported [27]. In accordance to the literature, PLGA solely was used, up to date, only for coating of the bare UCNPs through intercalation process, but obtained biocompatible particles sized around 250 nm exhibited negligible cellular uptake and mild cytotoxicity (cellular viability of about 80%) when applied at concentration of 62.5 μg/mL to the human keratinocyte and fibroblast cells [28].

In this study, a new kind of hybrid NaYF4:Yb,Er/PLGA nanoparticles for efficient cell labeling was prepared through one-pot solvothermal synthesis using non-toxic reagents. Hence, PLGA functional groups attached *in situ* to the UCNPs surface ensure excellent biocompatibility without compromising upconverting process. Furthermore, NaYF4:Yb,Er/PLGA UCNPs demonstrated dose-dependent cytotoxicity against oral squamous cell carcinoma (OSCC) without damaging healthy non-cancerous human gingival cells (HGC), so could be considered as promising and reasonably safe candidate for theranostic.

2. Materials and methods

2.1. Synthesis and characterization of $NaYF_4$:Yb,Er/PLGA UCNPs

All of the chemicals used for PLGA mediated solvothermal synthesis of $NaY_{0.8}Yb_{0.17}Er_{0.03}F_4$ were purchased from Sigma-Aldrich. Deionized water was used throughout. Defined stoichiometric amounts of rare earth nitrates (5 mmol in total) were dissolved in 15 ml of deionized water and then mixed with 5 ml of NaF solution (1.75-fold excess) and 0.1 g of PLGA (lactide:glycolide, 75:25; Mr. 66,000–107,000) dissolved in 40 ml of acetone. Obtained mixture was stirred for 15 min, transferred to 100 ml Teflon lined autoclave and sealed. Since that PLGA is thermally stable until 250 °C under atmospheric pressure [29] synthesis was carried out at twice lower temperature of 120 °C with a continual stirring (100 rpm) for 24 h. After cooling, the as-prepared NaYF4:Yb,Er/PLGA UCNPs were washed with acetone by centrifuging (8000 rpm, 10 min) and dried at 80 °C for 3 h.

The NaYF4:Yb,Er/PLGA UCNPs were characterized by the X-ray powder diffraction (XRPD) using Bruker D8 Discovery equipped with a Cu-Kα source (λ = 1.5406 Å). The pattern was recorded with a step scan of 0.02° and accounting time of 5 s per step. Powders microstructural data were acquired through combined La Bail and Rietveld refinement in Topas 4.2 software. For cubic α- and hexagonal β-$NaYF_4$ phase refinements were carried out in *Fm-3m* (No. 225) and *P63/m* (No. 176) space groups, respectively. The morphological features of the as-prepared particles were investigated by means of both, scanning and transmission electron microscopy (JEOL JSM-6701F SEM and JEOL JEM 2010 TEM operating at 200 kV at phase contrast and selected area electron diffraction (SAED) modes) coupled with energy dispersive spectroscopy (EDS). For the aforementioned analyses the particles were suspended in isopropyl alcohol and dropped directly on the stub (for SEM) or on lacey carbon film supported on a Cu grid after 20 min sonication (for TEM). The SemAfore 5.21 JEOL software was used to construct particle size distribution diagrams, while Fourier processing of high resolution TEM images was performed with Digital Micrograph 3.7.4 Gatan Inc. software. Detection of the PLGA ligands on the particles surface was done by Fourier transform infrared spectroscopy (FTIR) using Thermo Scientific Nicolet 6700 spectrophotometer (Thermo Fisher Scientific) with a Smart iTR Diamond Attenuated Total Reflectance accessory. Spectra were recorded using typically 128 scans at the resolution of 4 cm^{-1}. Dynamic light scattering measurements of

the UCNPs hydrodynamic radius (R$_H$) were performed on a Malvern Zetasizer Nano ZS in the de-ionized water and medium used for testing of the cell viability and imaging. For that purpose, NaYF$_4$:Yb,Er/PLGA UCNPs were dispersed at the concentration of 1 mg/ml and passed through a 0.45 µm cellulose syringe filter before DLS measurements. Photoluminescence emission measurement was performed at room temperature using Spex Fluorolog with C31034 cooled photomultiplier under diode laser excitation at 980 nm. From obtained spectrum the chromaticity coordinate calculation was done.

2.2. OSCC and HGC cultures

Human tumor and healthy gingival tissues were obtained from the patients at the Clinic of Maxillofacial Surgery of School of Dental Medicine, University of Belgrade immediately after the surgery, with signed informed consent approval from each patient prior to study participation. The planning experiments were approved by the Ethical Committee of the School of Dental Medicine (36/31), University of Belgrade.

Tumor tissues were oral squamous cell carcinoma (OSCC) of a tongue. Preparation of the cell cultures was performed using slightly modified procedure of Pozzi et al. [30]. Dulbecco's Modified Eagle Medium (DMEM) supplemented with 20% fetal bovine serum (FBS) and 100 U/ml penicillin-streptomycin (Sigma-Aldrich, St. Louis, USA) was used to transport the tissue sample. The tissue samples were minced with blades into small pieces. The cells were grown in DMEM supplemented with 10% FBS and 100 U/ml penicillin-streptomycin seeded onto T25 cell culture flasks. The cells were maintained at 37 °C in humidified atmosphere containing 5% CO$_2$. The medium was changed every 2–3 days and the cells were passaged prior to reaching 80% confluence. To avoid fibroblast contamination in cultures, brief exposure to TrypLE Express (Thermo Fisher Scientific, Waltham, USA) was used. OSCC used for the present study were obtained after the third passage.

Human gingival tissues were obtained from three different, healthy patients, aged 19–25 years, during extraction of the impacted third molar. The gingival tissue was transported in Gibco Dulbecco's modified Eagle's F12 medium (D-MEM/F12; Thermo Fisher Scientific), supplemented with 20% FBS and 1% antibiotic/antimycotic (ABAM; Thermo Fisher Scientific) solution. The gingival tissue was rinsed in phosphate-buffered saline (PBS) from Sigma-Aldrich (St. Louis, USA) and subjected to outgrowth isolation method. Tissue was minced into approximately 1 mm^2 fragments, and placed in 25-cm^2 culture flasks with DMEM/F12 supplemented with 10% FBS and 1% ABAM, and incubated at 37 °C in 5% CO$_2$. The cells were allowed to reach 80% confluence prior to passage. The culture medium was changed every 2–3 days. HGC after the second passage were used in this study.

2.3. MTT assay

For assessment of cytotoxicity, NaYF$_4$:Yb,Er/PLGA UCNPs suspensions with three different concentrations (10, 25 and 50 µg/ml) were prepared. For each concentration, adequate mass of NaYF$_4$:Yb,Er/PLGA UCNPs was aseptically weighted and suspended in sterile water, shaken vigorously and sonicated for 3 min. OSCC and HGC were seeded in a 96-well plate (10,000 cells per well) and incubated at 37 °C in humidified 5% CO$_2$ atmosphere. After 24 h hours 100 µl of the NaYF$_4$:Yb,Er/PLGA UCNPs were added (10, 25 or 50 µg/ml) in each plate. Incubation with the cell cultures was stopped after 24 h by discarding of spent media, and medium containing 3-(4,5-dimethylthiazol-2-yl)-2,5 diphenyltetrazolium bromide (MTT, 0.5 mg/ml) (Sigma-Aldrich, St. Louis, USA) was added to each well and than incubated for additional 4 h, as previous described by Castiglioni et al. [31]. The supernatant was discarded and formazan crystals were dissolved in 100 µl dimethyl sulfoxide (DMSO) (Sigma-Aldrich, St. Louis, USA) by shaking in duration of 20 min at 37 °C. Optical density was measured at 540 nm using ELISA
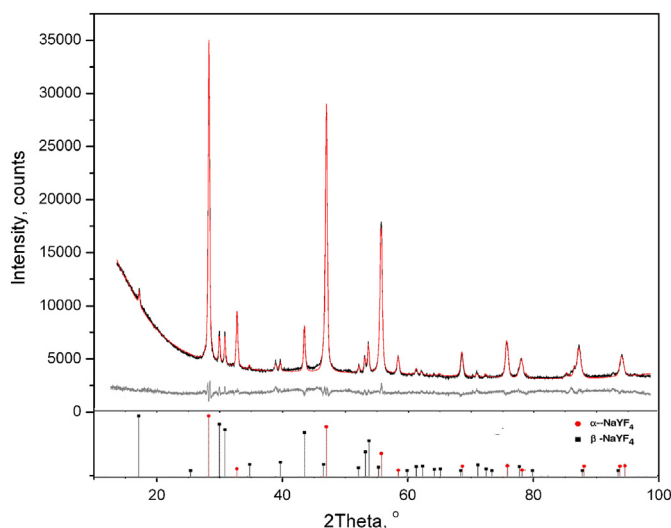

Fig. 1. XRPD pattern of NaYF$_4$:Yb,Er/PLGA UCNPs (black), refined structure (red) and difference curve (gray); Standard patterns of cubic (PDF 01-077-2042) and hexagonal (PDF 01-016-0334) NaYF$_4$ phase are given as bottom bar line diagram. (For interpretation of the references to color in this figure legend, the reader is referred to the web version of this article.)

microplate reader (Enzyme-linked immunosorbent assay) RT-2100c, Rayto, China). Three wells without NaYF$_4$:Yb,Er/PLGA UCNPs were used as a control group.

2.4. Statistical analysis

According to the cytotoxicity test procedure, the experiments were performed in triplicate and repeated three times in the independent experiments. Cells viability, expressed by the ratio of absorbance of the cells incubated with UCNPs to that of the cells incubated with culture medium only, were given in diagram as the mean ± standard deviation (SD).

2.5. Cells imaging by laser scanning microscopy

For the visualization of NaYF$_4$:Yb,Er/PLGA UCNPs uptake, the lowest concentration of NaYF$_4$:Yb,Er/PLGA UCNPs suspension (10 µg/ml) was filtered through 0.45 µm syringe filter to separate large agglomerates and to avoid saturation during visualization. Filtered solution was used further for incubation with cells and preparation of samples for laser scanning microscopy. Sterilized 22 mm × 22 mm glass coverslips were placed in 6-well plates, and 10,000 of OSCC and HGC were seeded per coverslip and incubated at 37 °C in humidified atmosphere containing 5% CO$_2$. The next day cells were exposed to NaYF$_4$:Yb,Er/PLGA UCNPs solution and incubated for another 24 h. Coverslips with adherent cells were gently rinsed with PBS twice and fixated with 4% paraformaldehyde (PFA) (Sigma-Aldrich, St. Louis, USA) for 20 min. Residuals of PFA were washed by PBS (3 × 3 min), coverslips were dried, 10 µl of Mowiol (Sigma-Aldrich, St. Louis, USA) was placed on fixated cells, and coverslips were placed on microscopic slides with cells positioned in between. Samples were stored in a dark until they were observed under confocal microscopy.

The homemade nonlinear laser scanning microscope used in this study was described in detail elsewhere [32]. Ti:Sapphire laser (Coherent, Mira 900-F) was used as a laser light source. It operates in two regimes. The first regime generates femto-second (FS) pulses at 730 nm convenient for unlabeled cell imaging since that enables two photon excitation of auto-fluorescence in cells. Note that two photon excitation here is considered as excitation of the molecule with no intermediate levels between ground and excited state and it is not related to
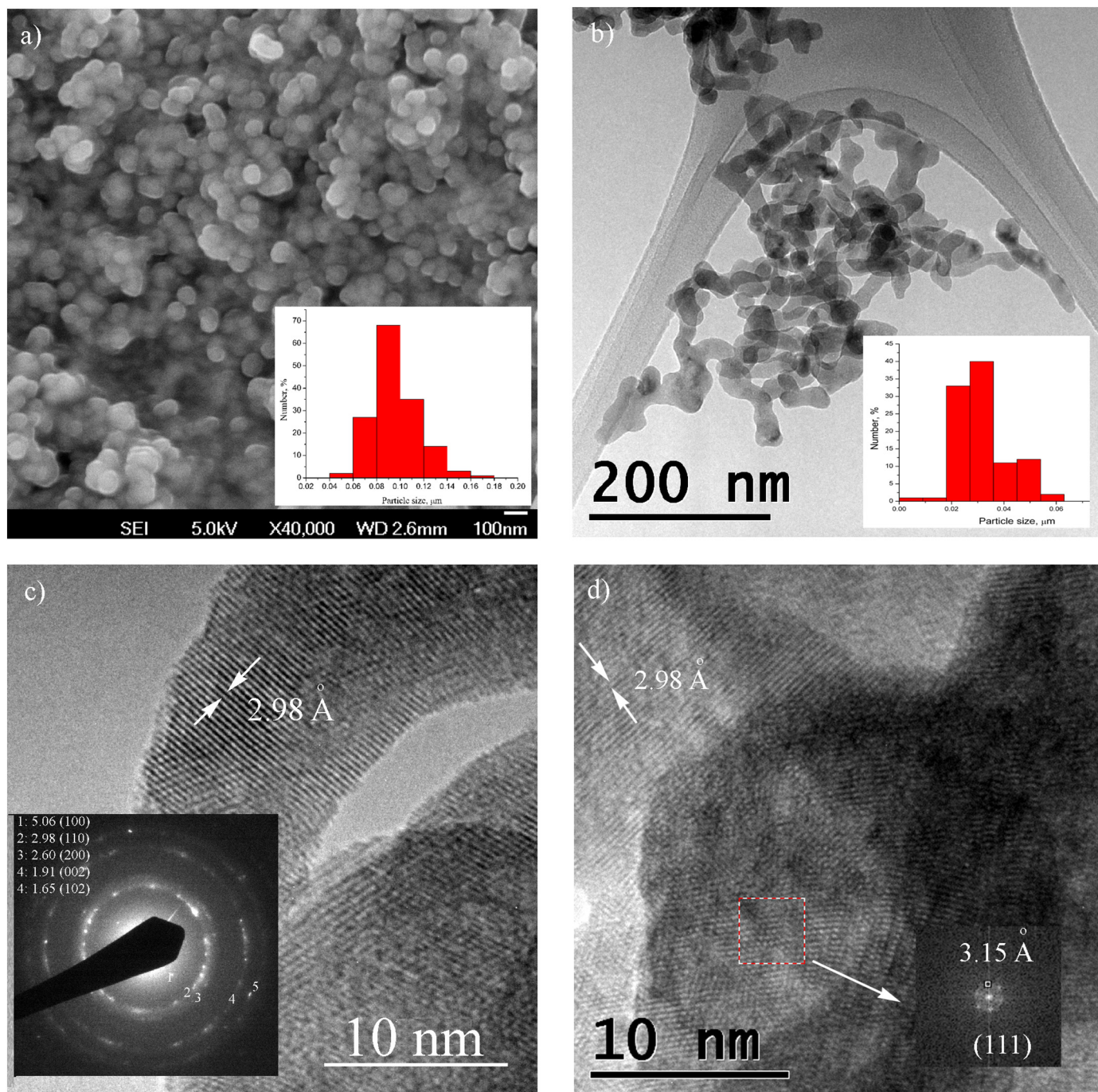
Fig. 2. SEM (a) and TEM (b–d) images of NaYF$_4$:Yb,Er/PLGA UCNPs. Corresponding particle size distribution histograms are given as insets in a and b; SAED inset in c represents d values of the interplanar spacing of hexagonally crystallized elongated nanoparticles, while FFT (inset in d) confirms cubic crystal cell arrangements in a spherical ones.

upconversion process. The second regime comprises generation of continuous wave (CW) radiation at 980 nm and was used for the excitation of NaYF$_4$:Yb,Er/PLGA UCNPs in cells. Due to the long UCNPs lifetime, the scanning rate was reduced during imaging in order to extend pixel dwell time. Hence the pixel dwell time was several times longer than fluorescence lifetime. Each fixed cell culture was imaged using Carl Zeiss, EC Plan-NEOFLUAR, 40 × 1.3 oil immersion objective for laser focusing and collection of the fluorescence. A visible interference filter (415 nm–685 nm) positioned in front of detector is used to remove scattered laser light. Thus, the whole visible range has been detected either for auto-fluorescence from cells or up-conversion from NaYF$_4$:Yb,Er/PLGA UCNPs in cells.

3. Results and discussion

3.1. Structural and morphological properties of NaYF$_4$:Yb,Er/PLGA UCNPs

To confirm the composition and the crystallinity of the synthesized NaYF$_4$:Yb,Er/PLGA UCNPs XRPD analysis was performed. Pattern presented in Fig. 1. reflects that obtained sample is a mixture of well crystallized cubic (*Fm-3m*) and hexagonal (*P63/m*) phase since all of the reflections, *i.e.* their positions and intensities, are in a good agreement with the reported 01-077-2042 and 01-016-0334 ICDD data, presented as bottom bar line diagram in the same figure. In general, NaYF$_4$ material has three different polymorphs: low temperature cubic, hexagonal
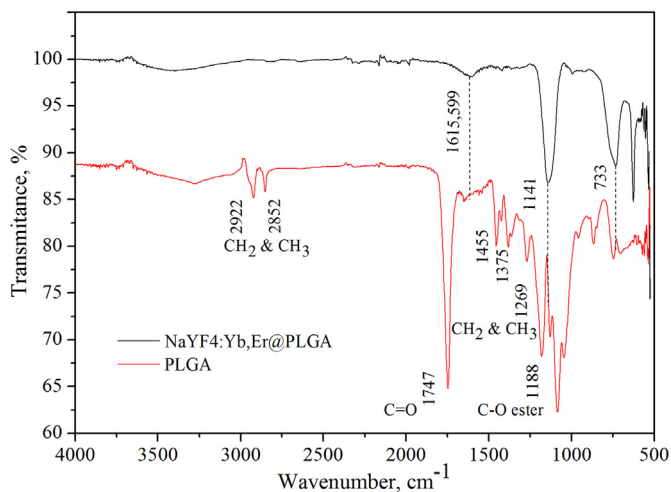
Fig. 3. FTIR of pure PLGA and NaYF$_4$:Yb,Er/PLGA UCNPs.

Fig. 5. MTT assay comparing viability of OSCC and HGC incubated with NaYF$_4$:Yb,Er/PLGA UCNPs for 24 h.

and high-temperature cubic – whose structure lacks detailed characterization [33]. In a low- temperature cubic phase (*Fm-3m*) there is only one site coordinated by eight fluoride anions over which Na$^+$ and RE^{3+} ions are randomly distributed in the cationic sub-lattice, whereas in the hexagonal (*P63/m*) there are two types of low-symmetry sites at which dopants could be arranged. As it is indicated recently, high-temperature cubic phase could be described with the same space group as a low-temperature one, but with the well-ordered distribution of sodium and RE cations [34]. The unit cell parameters of low-temperature cubic phase and hexagonal one crystallized in the NaYF$_4$:Yb,Er/PLGA sample were determined from XRPD data to be (Å): a = 5.4764(1); and a = 5.9785(3), c = 3.5088(4); respectively. Since cubic phase prevails in the sample (~85 wt%), refinement of this phase was performed starting from the ICSD 6025 card data. Decreased occupation of the cation site by Na$^+$ and Y^{3+} of 0.98(1) and 0.76(1) corresponds well with a nominal compound stoichiometry, while R$_{Bragg}$ value of 1.79 reflects good compliance with the structural model used during refinement. The average crystallite size of 33(1) nm was calculated using volume weighted mean column height broadening
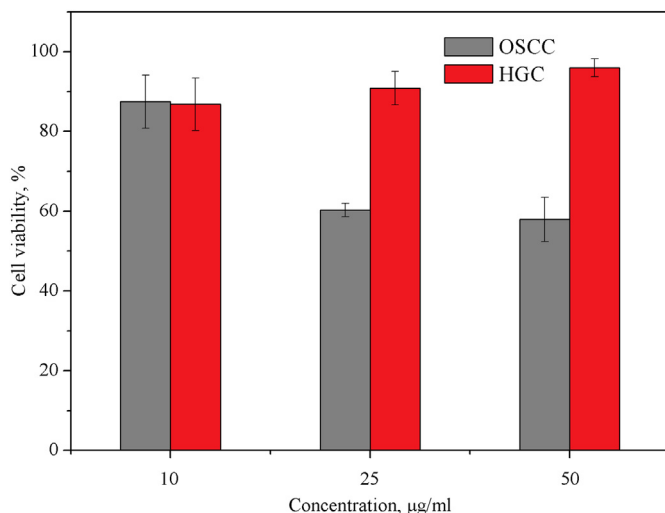
modeled by a Voigt function while Gaussian microstrain distribution was determined to be 0.113(4).

The morphological characteristic of the NaYF$_4$:Yb,Er/PLGA UCNPs were evaluated based on SEM and TEM analysis, Fig. 2. As presented in Fig. 2a, sample is composed of uniform and well defined spherical particles with average size around 100 nm. Backscattered electron images and EDS chemical analysis (not presented) implied compositional homogeneity and high particles purity. As it is notable from SEM, particles are stick together due to the PLGA presence. TEM analysis revealed existence of smaller nanoparticles with elongated shape and length up to 60 nm, Fig. 2b. The high resolution TEM image presented at Fig. 2c, exposes their good crystallinity, clear lattice fringes and the interplanar spacing of 2.98 Å which might be associated with a (110) plane of hexagonal phase. Furthermore, diffraction pattern *via* SAED mode presented as inset at the same figure pointed out that all of determined *d* values are consistent with the interplanar spacings of the hexagonal NaYF$_4$ phase (PDF 01-016-0334) confirming results derived
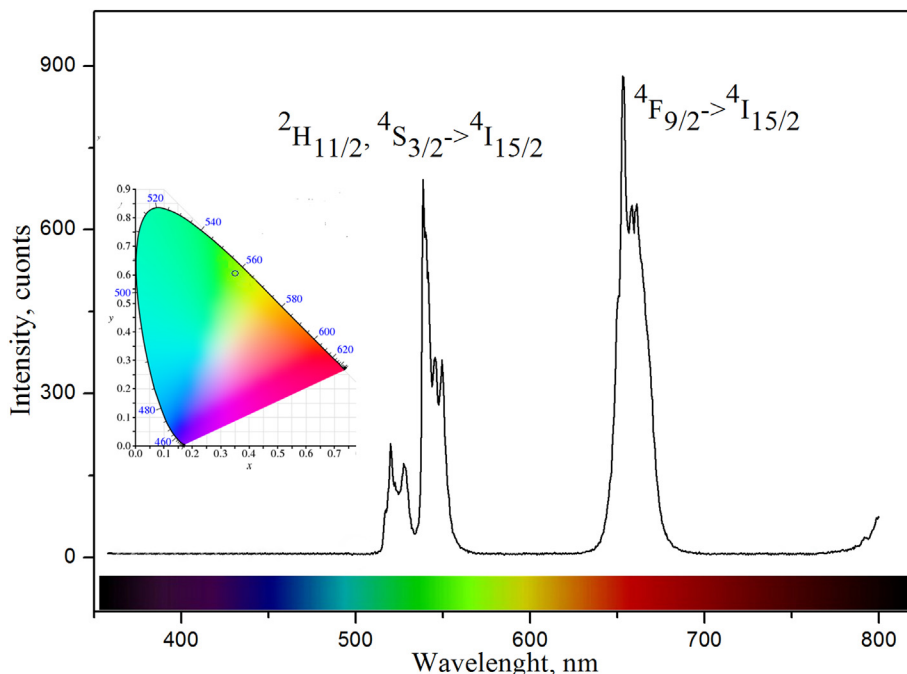

Fig. 4. Up-converted spectrum of NaYF$_4$:Yb,Er/PLGA UCNPs excited at 980 nm and corresponding CIE diagram (given as inset).
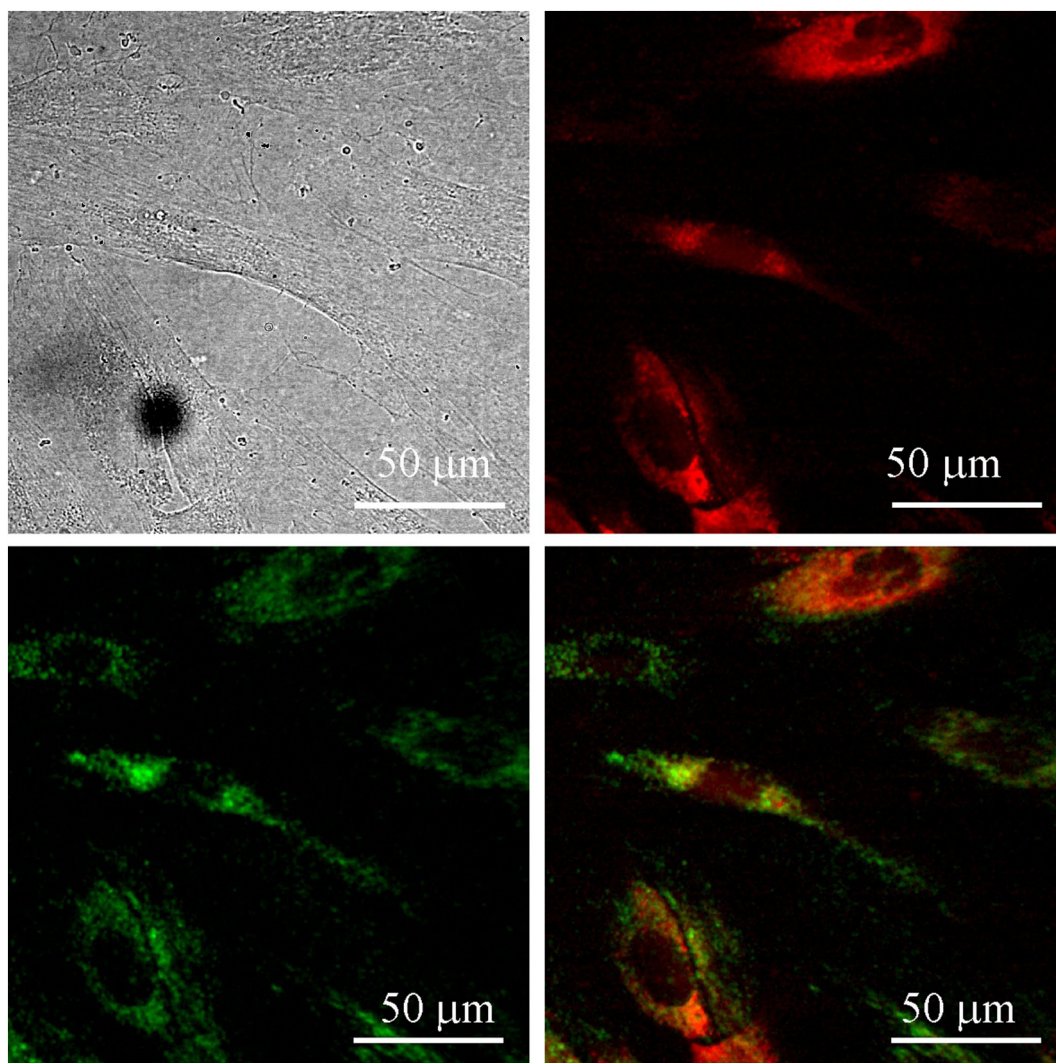
Fig. 6. Images of OSCC following 24 h incubation with 10 μg/ml of NaYF$_4$:Yb,Er/PLGA: bright field (top-left) and cells auto-fluorescence upon femto-second excitation at 730 nm (top-right), pseudo color image of the NaYF$_4$:Yb,Er/PLGA UCNPs upon CW excitation at 980 nm (bottom-left) and their positioning in cells, revealed through co-localization of the cell auto-fluorescence and the UCNPs emission (bottom-right). (For interpretation of the references to color in this figure legend, the reader is referred to the web version of this article.)

from XRPD. Cubic NaYF$_4$ phase was detected in somewhat smaller nanoparticles with a spherical shape, as it is shown in Fig. 2d. Confined growth of NaYF$_4$ nanocrystals was presumably caused by the interaction between the lanthanide ions and the carboxyl end groups of PLGA, which presence is verified further by FTIR analysis.

Colloidal size, polydispersity index (PDI) and stability of the NaYF$_4$:Yb,Er/PLGA UCNPs solutions were estimated from dynamic light scattering measurements, Fig. S1. While a monomodal size distribution was obtained in water (due instant agglomeration of the nanoparticles sized below 20 nm), the bimodal one was preserved in a medium over time (24 h). As a result, slightly higher average hydrodynamic diameter (R$_{Hav}$) of the NaYF$_4$:Yb,Er/PLGA UCNPs was detected in water (177 nm, PDI 0.32) than in medium (127 nm, PDI 0.31). Minimal changes distinguished after 1 h, confirms good stability of both colloids (195 nm, PDI 0.32; and 127 nm, PDI 0.31; in water and medium, respectively). With prolongation of time, after 24 h, magnitude of the NaYF$_4$:Yb,Er/PLGA UCNPs R$_{Hav}$ in water increased to 488 nm (PDI 0.3), while stayed unchanged in medium which is further used for cells bioimaging (122 nm, PDI 0.34).

Infrared absorption spectra of pure PLGA and NaYF$_4$:Yb,Er/PLGA UCNPs were recorded and presented at Fig. 3. Pure PLGA exhibited characteristic absorption bands which are classified in accordance to

the literature [35] as follows: CH$_3$ and CH$_2$ asymmetric stretching at 2850 and 2920 cm^{-1} respectively; C$=$O stretching around 1750 cm^{-1}, CH$_3$ and CH$_2$ symmetric angular deformation in the 1500–1250 cm^{-1} region and C$-$O ester stretching in the 1300–1150 cm^{-1} region. FTIR analysis of NaYF$_4$:Yb,Er/PLGA UCNPs revealed a decreased PLGA absorption due to side-chain vibrations as well as low-frequency shifting of its most intense band associated to the C$=$O stretching, which might be due to the carboxylic acid salts formation, O$=$C$-$ONa, as it was suggested in the literature [36]. This evident that applied synthesis method preserves the highly reactive carboxylic acid groups on UCNPs surface which is very important for their conjugation with biomolecules containing $-$NH$_2$ group, like antibodies, streptavidin and DNA, creating in that way carriers with high binding potential for targeted imaging and therapy [13].

3.2. Optical properties of NaYF$_4$:Yb,Er/PLGA UCNPs

The upconversion spectrum of NaYF$_4$:Yb,Er/PLGA UCNPs is presented in Fig. 4. Following excitation with 980 nm into the $^2F_{5/2}$ state of Yb^{3+} and subsequent energy transfer from Yb^{3+} to Er^{3+} ions (and *vice versa*), three distinct Er^{3+} emission bands centered at 520, 539 and 653 nm are clearly observed in the visible part of spectrum. The double
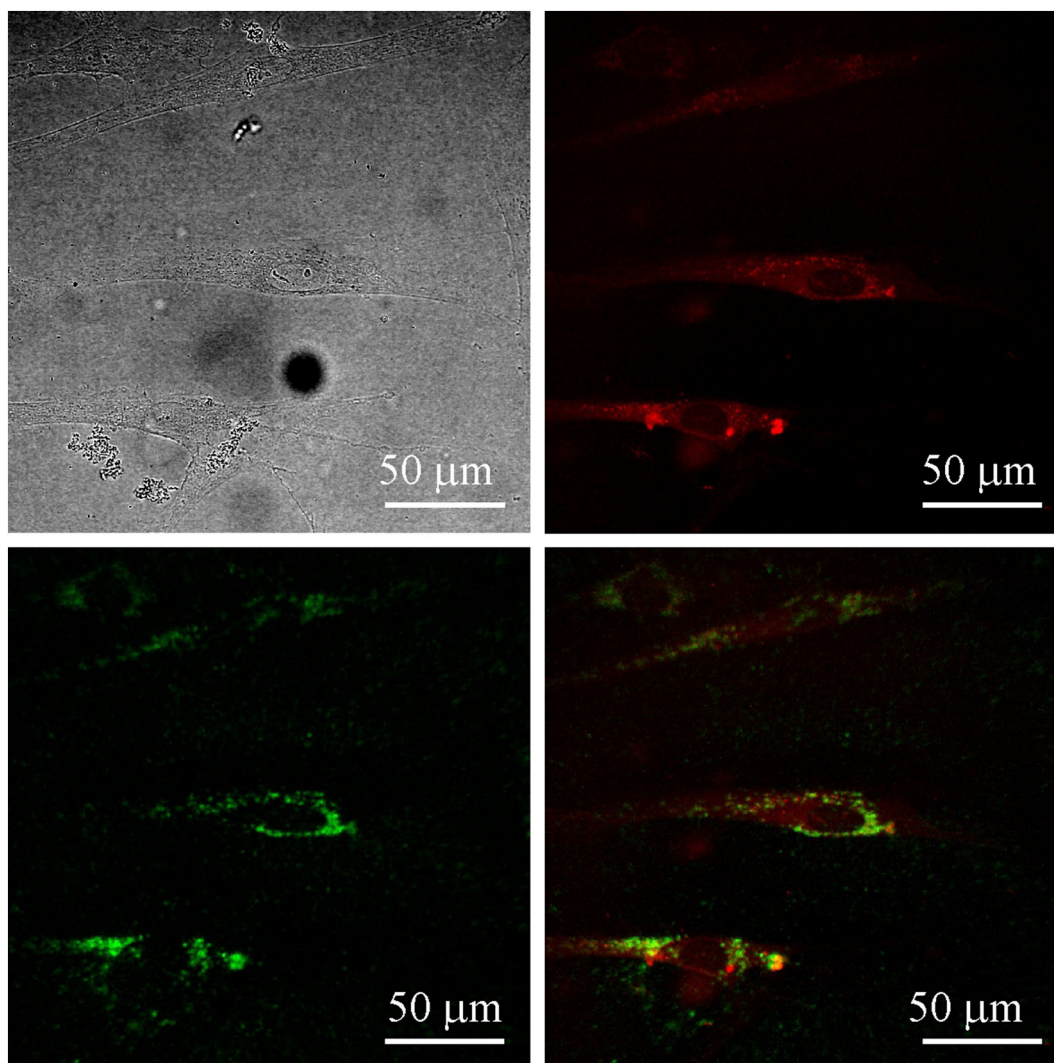
Fig. 7. Images of HGC following 24 h incubation with 10 µg/ml of NaYF$_4$:Yb,Er/PLGA: bright field (top-left) and cells auto-fluorescence upon femto-second excitation at 730 nm (top-right), pseudo color image of the NaYF$_4$:Yb,Er/PLGA UCNPs upon CW excitation at 980 nm (bottom-left) and their positioning in cells, revealed through co-localization of the cell auto-fluorescence and the UCNPs emission (bottom-right). (For interpretation of the references to color in this figure legend, the reader is referred to the web version of this article.)

green emissions between 512 and 533 nm and between 533 and 560 nm are attributed to the $^2H_{11/2} \rightarrow {}^4I_{15/2}$ and $^4S_{3/2} \rightarrow {}^4I_{15/2}$ transitions respectively, while a red emission observed between 630 and 690 nm is due to the $^4F_{9/2} \rightarrow {}^4I_{15/2}$ transition. Green band emission at 539 nm, characterized by several narrow lines associated with a splitting of the $^4S_{3/2}$ energy level by the matrix electric field, reflects the homogeneous distribution of Er^{3+} in the NaYF$_4$ phase [20]. On the other hand, the red emission appears due to a direct population of $^4F_{9/2}$ level from $^4I_{13/2}$ level (following the non-radiative decay from $^4I_{11/2}$ level which is intensified in nanocrystals) and a non-radiative relaxation from $^4F_{7/2}$ through the $^2H_{11/2}$ and $^4S_{3/2}$ levels. As a result, the integrated green to red emission ratios of 0.62 and CIE of (0.37, 0.61) determines the final color output of NaYF$_4$:Yb,Er/PLGA UCNPs, Fig. 4. Photostability of the NaYF$_4$:Yb,Er/PLGA UCNPs emission was also traced during 1 h, Fig. S2. As one could see, exceptionally stable UC luminescence signal was recorded.

3.3. Cytotoxicity of NaYF$_4$:Yb,Er/PLGA UCNPs

The viability of HSCC and HGC after 24 h exposure to NaYF$_4$:Yb,Er/PLGA UCNPs at concentrations of 10, 25 and 50 µg/ml, expressed in terms of percentages compared to the surviving cells in the control group is presented at Fig. 5. As it is notable from Fig. 5, the viability of HGC was highly preserved after 24 h exposure, being above 88% for all examined concentrations of NaYF$_4$:Yb,Er/PLGA UCNPs. At the same time, the tolerance of OSCC was found variable with the increase of NaYF$_4$:Yb,Er/PLGA UCNPs concentration. Only in the case of the lowest concentration viability of OSCC implied non-significant cytotoxicity of 89%, while higher NaYF$_4$:Yb,Er/PLGA concentrations exerted in them certain level of cytotoxicity, *i.e.* cell viability of only 60% was detected. This is quite surprising since cancer cells are usually highly resistant to therapeutics. Obtained data regarding preserved viability of HGC corroborated well by recent conclusions about cytotoxicity of bare and PLGA coated NaYF4:Yb:Er UCNPs tested on human skin cells [28]. Guller et al. [28] used the solvent evaporation technique for posterior formation of PLGA shell over the NaYF$_4$:Yb/Er nanoparticles that have been synthesized through decomposition of rare earth trifluoroacetates in oleic acid/octadecene mixture. Although the authors reported much lower internalization capacity, higher sensitivity of keratinocytes than of fibroblasts has been achieved, emphasizing the importance of studying normal cells. As it will be shown latter, maintaining of the high HGC viability in this study is not a consequence of the lower internalization of NaYF$_4$:Yb,Er/PLGA UCNPs in them, so evaluated differences in OSCC viability indicates that synthesized UCNPs could be

useful in therapeutic treatments of cancer cells.

3.4. In vitro laser scanning microscopy imaging of OSCC and HGC

For the evaluation of the NaYF$_4$:Yb,Er/PLGA UCNPs capability to be internalized in OSCC and HGC, the lowest NaYF$_4$:Yb,Er/PLGA UCNPs concentration of 10 μg/mL has been used. For this concentration, no significant cytotoxicity has been observed in both OSCC and HGC (Section 3.3) and therefore, it could be considered as the most promising concentration for diagnostic purpose.

Visualization of the OSCC and HGC labeled with the NaYF$_4$:Yb,Er/PLGA UCNPs was done using of a safe 980 nm laser intensity of 6 and 7.5 mW, respectively. The size of the imaged region was approximately 200 × 200 μm^2. Images of the OSCC are shown in Fig. 6. The top row, left panel shows bright field image of the sample. A pseudo color image of the cells auto-fluorescence upon femto-second excitation at 730 nm is shown in top-right panel. Bottom row - left panel shows the pseudo color image of the NaYF$_4$:Yb,Er/PLGA UCNPs upon CW excitation at 980 nm. Overlapping of the latter two images clearly implicates that observed fluorescence spots are related to the non-specific uptake of UCPNs through cell membrane and their positioning in a cytoplasmic area around cells nuclei. Size of the fluorescence spots indicates UCNPs aggregation in cells.

The consistent finding of the UCNPs internalization in the HGC has been drawn from Fig. 7, which presents HGCs labeled in the same way as OSCC. The fact that UCNPs are mainly localized in the vicinity of the cells nuclei, without visible entering in, designates that UCNPs didn't provoke gene disruption. In order to show comparable level of the NaYF$_4$:Yb,Er/PLGA UCNPs internalization in OSCC and HGC, quantification of the UCNPs signal from the Figs. 6 and 7, as well as additional one which show labeling of a single OSCC were done, and results obtained are presented in Supplement File (Figs. S3 and S4). Significant cellular internalization of NaYF$_4$:Yb,Er/PLGA UCNPs coupled with the preserved cells viability indicates that these could be useful theranostics for oral cavity cancers.

As it is pointed out before, the amount of literature showing cells viability and labeling with UCNPs is respectable and summarized in many reviews, but great majority is focused on cancer cells testing. At the same time, data about mucosal cytotoxicity and drug deliver capacity of UCNPs tested on primary cultures and normal cells are limited and inconsistent in achieved results due to the considerable disparity of the UCNPs characteristics and type of protective organic shell used [37–39]. Thus, it is not easy to compare these with data presented in this study but it is worth to note that realistic UCNP-assisted imaging depth nowadays is estimated to be up to 1 cm [28], which corresponds well with the depth of skin and mucosa, so successful OSCC and HGC labeling with NaYF$_4$:Yb,Er/PLGA UCNPs holds promise for these to be used as theranostic agents in the future.

4. Conclusion

In conclusion, we have demonstrated the successful fabrication of the new NaYF$_4$:Yb,Er/PLGA UCNPs that could be used as probes for NIR-excited fluorescence (in vitro) imaging of human mucosal cells. Comprehensive morphological and structural analyses implied crystallization of a low-temperature cubic phase in spherical nanoparticles (~100 nm), as well as, hexagonal one in elongated nanocrystals (~60 nm). As a consequence of the upconversion, green emission (between 512 and 533 nm and between 533 and 560 nm) and red emission (between 630 and 690 nm) are both prominent in spectra, yielding a final light green output (CIE 0.37, 0.61). PLGA functional groups present at NaYF$_4$:Yb,Er UCNPs surface make them accessible for further conjugation with biologically important molecules, while in the present form enable non-specific cellular uptake without compromising cells viability. Moreover, evidences about lower cytotoxicity under significant internalization of NaYF$_4$:Yb,Er/PLGA UCNPs in the vicinity of

the cell nucleus without gene disrupting, represent an important step toward application of UCNP-based particles for diagnosis or the treatment of cancer cells.

Appendix A. Supplementary data

Supplementary data to this article can be found online at https://doi.org/10.1016/j.msec.2018.05.081.

References

[1] N. Vigneswaran, M.D. Williams, Epidemiological trends in head and neck cancer and aids in diagnosis, Oral Maxillofac. Surg. Clin. North Am. 26 (2) (2014) 123–141.
[2] A.K. Markopoulos, Current aspects on oral squamous cell carcinoma, Open Dent. J. 6 (2012) 126–130.
[3] J.H. Wang, B. Wang, Q. Liu, Q. Li, H. Huang, L. Song, T.Y. Sun, H. Wang, X.F. Yu, C. Li, P.K. Chu, Bimodal optical diagnostics of oral cancer based on Rose Bengal conjugated gold nanorod platform, Biomaterials 34 (2013) 4274–4283.
[4] P. Padmanabhan, A. Kumar, S. Kumar, R.K. Chaudhary, B. Gulyás, Nanoparticles in practice for molecular-imaging applications: an overview, Acta Biomater. 41 (2016) 1–16.
[5] X. Huang, J. Lin, Active-core/active-shell nanostructured design: an effective strategy to enhance Nd^{3+}/Yb^{3+} cascade sensitized upconversion luminescence in lanthanide-doped nanoparticles, J. Mater. Chem. C 3 (2015) 7652–7657.
[6] K. Presley, J. Hwang, S. Cheong, R. Tilley, J. Collins, M. Viapiano, J. Lannutti, Nanoscale upconversion for oxygen sensing, Mater. Sci. Eng. C 70 (2017) 76–84.
[7] X. Zhu, Q. Su, W. Feng, F. Li, Anti-stokes shift luminescent materials for bio-applications, Chem. Soc. Rev. 46 (2017) 1025–1039.
[8] H. Dong, L.D. Sun, C.H. Yan, Energy transfer in lanthanide upconversion studies for extended optical applications, Chem. Soc. Rev. 44 (2015) 1608–1634.
[9] P. Zhao, W. Ji, S. Zhou, L. Qiu, L. Li, Z. Qian, X. Liu, H. Zhang, X. Cao, Upconverting and persistent luminescent nanocarriers for accurately imaging-guided photothermal therapy, Mater. Sci. Eng. C 79 (2017) 191–198.
[10] B. Hou, W. Yang, C. Dong, B. Zheng, Y. Zhang, J. Wu, H. Wang, J. Chang, Controlled co-release of doxorubicin and reactive oxygen species for synergistic therapy by NIR remote-triggered nanoimpellers, Mater. Sci. Eng. C 74 (2017) 94–102.
[11] S. Chen, C. Zhang, G. Jia, J. Duan, S. Wang, J. Zhang, Size-dependent cytotoxicity of europium doped NaYF4 nanoparticles in endothelial cells, Mater. Sci. Eng. C 43 (2014) 330–342.
[12] X. Wu, G. Chen, J. Shen, Z. Li, Y. Zhang, G. Han, Upconversion nanoparticles: a versatile solution to multiscale biological imaging, Bioconjug. Chem. 26 (2015) 166–175.
[13] J. Zhou, Z. Liu, F. Li, Upconversion nanophosphors for small-animal imaging, Chem. Soc. Rev. 41 (2012) 1323–1349.
[14] G.K. Das, D.T. Stark, I.M. Kennedy, Potential toxicity of up-converting nanoparticles encapsulated with a bilayer formed by ligand attraction, Langmuir 30 (2014) 8167–8176.
[15] F. Wang, D.K. Chatterjee, Z. Li, Y. Zhang, X. Fan, M. Wang, Synthesis of poly-ethylenimine/NaYF4 nanoparticles with upconversion fluorescence, Nanotechnology 17 (2006) 5786–5791.
[16] M. Wang, C.-C. Mi, J.-L. Liu, X.-L. Wu, Y.-X. Zhang, W. Hou, F. Li, S.-K. Xu, One-step synthesis and characterization of water-soluble NaYF4:Yb,Er/Polymer nanoparticles with efficient up-conversion fluorescence, J. Alloys Compd. 485 (2009) L24–L27.
[17] T. Cao, Y. Yang, Y. Gao, J. Zhou, Z. Li, F. Li, High-quality water-soluble and surface-functionalized upconversion nanocrystals as luminescent probes for bioimaging, Biomaterials 32 (2011) 2959–2968.
[18] A. Sedlmeier, H.H. Gorris, Surface modification and characterization of photon-upconverting nanoparticles for bioanalytical applications, Chem. Soc. Rev. 44 (2015) 1526–1560.
[19] I. Dinic, M.E. Rabanal, K. Yamamoto, Z. Tan, S. Ohara, L.T. Mancic, O.B. Milosevic, PEG and PVP assisted solvothermal synthesis of NaYF4:Yb^{3+}/Er^{3+} up-conversion nanoparticles, Adv. Powder Technol. 27 (2016) 845–853.
[20] I. Dinic, S. Ohara, T. Koji, M.E. Rabanal, A.M. Costa, B.A. Marinkovic, L. Mancic, O. Milosevic, Compositional and structural dependence of upconverting RE-fluorides obtained through EDTA assisted hydrothermal synthesis, Adv. Powder Technol. 28 (1) (2017) 73–82.
[21] H.M. Mansour, M. Sohn, A. Al-Ghananeem, P.P. Deluca, Materials for pharmaceutical dosage forms: molecular pharmaceutics and controlled release drug delivery aspects, Int. J. Mol. Sci. 11 (2010) 3298–3322.
[22] H.K. Makadia, S.J. Siegel, Poly lactic-co-glycolic acid (PLGA) as biodegradable controlled drug delivery carrier, Polymer 3 (3) (2011) 1377–1397.
[23] F. Danhier, E. Ansorena, J.M. Silva, R. Coco, A. Le Breton, V. Préat, PLGA-based

nano particles: an overview of biomedical applications, J. Control. Release 161 (2) (2012) 505–522.

[24] R.N. Mariano, D. Alberti, J.C. Cutrin, S.G. Crich, S. Aime, Design of PLGA based nanoparticles for imaging guided applications, Mol. Pharm. 11 (2014) 4100–4106.

[25] J. Zhao, H. Yang, J. Li, Y. Wang, X. Wang, Fabrication of pH-responsive PLGA(UCNPs/DOX) nanocapsules with upconversion luminescence for drug delivery, Sci. Rep. 7 (2017) (Article No. 18014).

[26] S.J. Budijono, J. Shan, N. Yao, Y. Miura, T. Hoye, R.H. Austin, Y. Ju, R.K. Prud'Homme, Synthesis of stable block-copolymer-protected NaYF$_4$:Yb^{3+}, Er^{3+} up-converting phosphor nanoparticles, Chem. Mater. 22 (2010) 311–318.

[27] X. Bai, S. Xu, J. Liu, L. Wang, Upconversion luminescence tracking of gene delivery via multifunctional nanocapsules, Talanta 150 (2016) 118–124.

[28] A.E. Guller, A.N. Generalova, E.V. Petersen, A.V. Nechaev, I.A. Trusova, N.N. Landyshev, A. Nadort, E.A. Grebenik, S.M. Deyev, A.B. Shekhter, A.V. Zvyagin, Cytotoxicity and non-specific cellular uptake of bare and surface-modified upconversion nanoparticles in human skin cells, Nano Res. 8 (5) (2015) 1546–1562.

[29] R.M. Mainardes, M.P.D. Gremião, R.C. Evangelista, Thermoanalytical study of praziquantel-loaded PLGA nanoparticles, Braz. J. Pharm. Sci. 42 (4) (2006) 523–530.

[30] V. Pozzi, D. Sartini, R. Rocchetti, A. Santarelli, C. Rubini, S. Morganti, R. Giuliante, S. Calabrese, G. Di Ruscio, F. Orlando, M. Provinciali, F. Saccucci, L. Lo Muzio, M. Emanuelli, Identification and characterization of cancer stem cells from head and neck squamous cell carcinoma cell lines, Cell. Physiol. Biochem. 36 (2015) 784–798.

[31] S. Castiglioni, C. Caspani, A. Cazzaniga, J.A. Maier, Short- and long-term effects of silver nanoparticles on human microvascular endothelial cells, World J. Biol. Chem. 5 (2014) 457–464.

[32] K. Bukara, S. Jovanic, I.T. Drvenica, A. Stancic, V. Ilic, M.D. Rabasovic, D. Pantelic, B. Jelenkovic, B. Bugarski, A.J. Krmpot, Mapping of hemoglobin in erythrocytes and erythrocyte ghosts using two photon excitation fluorescence microscopy, J. Biomed. Opt. 22 (2) (2017) 026003(8 pages).

[33] T. Laihinen, M. Lastusaari, L. Pihlgren, L.C.V. Rodrigues, J. Holsa, Thermal behaviour of the NaYF$_4$:Yb^{3+},R^{3+} materials, J. Therm. Anal. Calorim. 121 (2015) 37–43.

[34] L. Wang, X. Li, Z. Li, W. Chu, R. Li, K. Lin, H. Qian, Y. Wang, C. Wu, J. Li, D. Tu, Q. Zhang, L. Song, J. Jiang, X. Chen, Y. Luo, Y. Xie, Y. Xiong, A new cubic phase for α NaYF$_4$ host matrix offering high upconversion luminescence efficiency, Adv. Mater. 27 (2015) 5528–5533.

[35] A.T.C.R. Silva, B.C.O. Cardoso, M.E.S.R. Silva, R.F.S. Freitas, R.G. Sousa, Synthesis, characterization, and study of PLGA copolymer in vitro degradation, J. Biomater. Nanobiotechnol. 6 (2015) 8–19.

[36] J.B. Lee, Y.G. Ko, D. Cho, W.H. Park, B.N. Kim, B.C. Lee, I.K. Kang, O.H. Kwon, Modification of PLGA nanofibrous mats by electron beam irradiation for soft tissue regeneration, J. Nanomater. (2015) 10, http://dx.doi.org/10.1155/2015/295807 (Article ID 295807).

[37] U. Bazylińska, D. Wawrzyńczyk, J. Kulbacka, R. Frąckowiak, B. Cichy, A. Bednarkiewicz, M. Samoć, K.A. Wilk, Polymeric nanocapsules with upconverting nanocrystals cargo make ideal fluorescent bioprobes, Sci. Rep. 6 (2016) 29746.

[38] H.C. Guo, R.Z. Hao, H.S. Qian, S.Q. Sun, D.H. Sun, H. Yin, Z.X. Liu, X.T. Liu, Upconversion nanoparticles modified with aminosilanes as carriers of DNA vaccine for foot-and-mouth disease, Appl. Microbiol. Biotechnol. 95 (2012) 1253–1263.

[39] L. Zhao, A. Kutikov, J. Shen, C. Duan, J. Song, G. Han, Stem cell labeling using polyethylenimine conjugated (α-NaYbF$_4$:Tm^{3+})/CaF$_2$ upconversion nanoparticles, Theranostics 3 (4) (2013) 249–257.